TERAHERTZ SENSING APPLICATION BY USING FRACTAL GEOMETRIES OF SPLIT-RING RESONATORS

Yanbing Ma[*]**, Huaiwu Zhang, Yuanxun Li, Yicheng Wang, and Weien Lai**

State Key Laboratory of Electronic Films and Integrated Devices, University of Electronic Science and Technology of China, Chengdu 610054, People's Republic of China

Abstract—In this study, we report the simulation, fabrication and characterization of a dual-band fractal metamaterial used for terahertz sensing application. By applying the fractal structures of square Sierpinski (SS) curve to the split-ring resonators (SRRs), more compact size and higher sensitivity can be achieved as privileges over conventional SRRs. The influence of different geometrical parameters and the order of the fractal curve on the performances are investigated. Then overlayers are added to the fractal SRRs in order to explore the performance of the entire system in terms of sensing phenomenon. The changes in the transmission resonances are monitored upon variation of the overlayer thickness and permittivity. Measured results show good agreement with simulated data. At the second resonance of the second-order SS-SRRs, maximum frequency shifts of 19.8 GHz, 26.3 GHz and 37.8 GHz were observed for a 2 μm, 4 μm and 10 μm thickness of photoresist. The results show good sensitivity of the sensors suggesting they can be used for a myriad of terahertz sensing applications in biology and chemistry.

1. INTRODUCTION

Artificial metamaterials (MTMs) have attracted much attention owing to their extraordinary features which are generally not found in nature. Since numerical and experimental studies of the first split-ring-resonator-based MTM structure in the microwave region [1–4], this kind of structure has been used in many applications such

as sensing [1, 3, 5], absorber [6–8], superlensing [9–11], and so on. With respect to sensing, MTMs have been proven to be good candidates in the THz regime for highly sensitive chemical or biological detection since the unit cell dimensions are typically sub-wavelength and frequency response can be tuned according to their shape and geometrical dimensions [12–14]. This means they can easily be made resonant at terahertz frequencies mainly by simple scaling. In addition, since they are arrayed and effectively homogenous structures, they are very easily probed with conventional terahertz time-domain spectroscopy (TDS). Recent studies show that fractal structures have arisen as candidates to make split-ring-resonator-based MTMs with interesting resonant properties not achievable in conventional MTMs [15–17]. In the detection techniques for sensing chemical or biological compounds, frequency shifts at two or three different resonant frequencies can enhance measurement accuracy and negate possible false-positive identifications [18]. However, to create multi-frequency resonance in the conventional planar MTMs, more than one unit cell that each has a distinct element are needed to added together to form a checkerboard pattern thus increasing some difficulties in analysis and manufacturing [19]. On the contrary, the fractal structure inherently can display multi-frequency operation within a single unit. In addition, due to the unique fractal characteristic of diverging boundary length within a finite area, it is possible to fabricate MTMs which are extremely small as compared to the wavelength at operational frequency [15].

In this paper, we investigate terahertz characteristics of SRRs combined with square Sierpinski (SS) fractal curve. Firstly, in Section 2, in order to analyze the influence of different geometrical parameters on the performance of the SS-SRRs with different fractal order, we simulated the structures using the commercial CST Microwave Studio 2011 with the frequency domain solver. The MTMs depicted in Fig. 1 were modeled as perfect conductor and Unit Cell boundary conditions were assigned on the lateral faces of the unit cell. Floquet ports on the other boundaries propagated a plane wave longitudinally on the MTMs surface. Then the frequency shifts as the thickness and permittivity of overlayer varies without a dielectric or lossy substrate are presented in order to analyze fundamental limitations of the MTM sensor. At last, the sensor based on quartz glass substrate with the dielectric constant of 3.75 and thickness of 130 μm is analyzed to reveal the influence of thick substrate on the sensitivity of the MTMs sensor. Two resonant frequencies can be observed in the transmission spectrum and the second resonant frequency is more sensitive to the variation of the overlayers. In
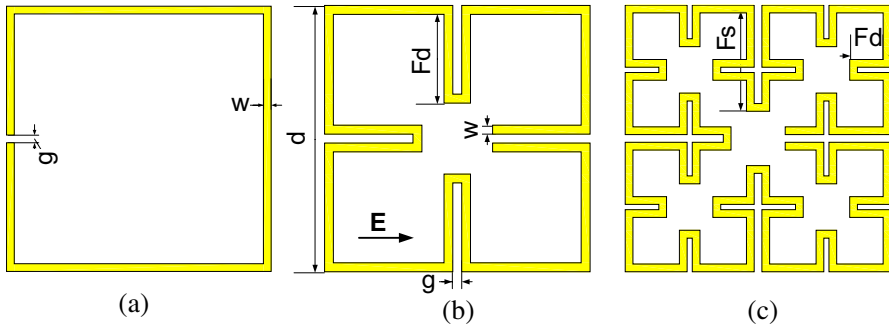
Figure 1. (a) Conventional SRR. (b) Square Sierpinski fractal curve of the second order. (c) Square Sierpinski fractal curve of the third order.

Section 3, the simulation and measurement results are given and good agreement have been achieved.

2. DESIGN AND ANALYSIS

2.1. Benefits from the Fractal SRRs

The fractal curves have been known since the end of 19th century, when Peano constructed a continuous curve that passes through every point of a given region. The fractal curves are characterized by fractal, i.e., non-integer dimension. The dimension of every fractal curve is the number between 1 and 2, and can be understood as a measure of the space-filling ability of the fractal curve.

Miniaturization has always been an ever-growing demand in component design. In the fractal structure, a boundary length diverges within a finite area as the fractal order increases to an infinite value. There is the possibility of fabricating components with sample sizes that are extremely small as compared to the convention structure at the same operational frequency.

In this paper, square Sierpinski fractal curve is adopted to form the split-ring resonator. Fig. 1 shows the schematic view of the conventional SRR and the unit-cell of the SS-SRRs with the geometrical dimensions and the considered orientation of the incoming electric field. In the simulation, the propagation direction is chosen to be perpendicular to the plane of the structure. The unit cell of each designs is square-shaped with the side length of $d = 300\,\mu$m, and lattice period of $p = 400\,\mu$m. Fd and Fs denote length of insets of SS-SRRs with different fractal order, respectively.

According to [20], with the electric field oriented perpendicularly to the SRR gap, two resonance can be observed. The first resonant frequency f_1 is originated from LC resonance, while the second resonant frequency f_2 is known as dipole resonance. However, when E is parallel to the SRR gap, there is only a single resonance which is analogous to the f_1 half wave resonance.

Under the condition of E paralleling to the gap as shown in Fig. 1, the resonances of fractal SS-SRR are also originated from the half wave resonance, which is similar to conventional SRRs. In addition, the multi-frequency operation can be attributed to the self-similar current distribution on the fractal surface [15, 21] as shown in Fig. 2(a).
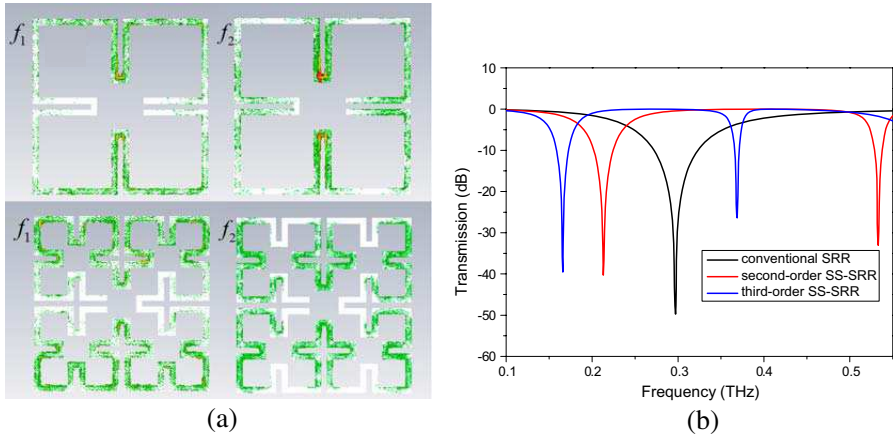

(a)   (b)

Figure 2. (a) Current distribution on the surface of fractal SRRs. (b) Transmission response of fractal SRRs and convention SRR when $E \parallel$ gap.

In Fig. 2(b), the first resonances can be observed at 0.297 THz, 0.213 THz and 0.166 THz for the conventional SRR, 2nd order SS-SRR and 3rd order SS-SRR respectively with occupying a same dimension. Such the red shift is attributed to the increase of the line length with increasing the fractal order. The meandered lines lengthen the path current flowing through, for resonant structures such as a dipole antenna, which means decreased operating frequency. These results reflect the fractal's characteristic of space-filling. So if operating at the same resonant frequency, the fractal structure with higher order will have more compact size.

We define the frequency shift as $\Delta f_H = f_H - f_0$, where f_H denotes the resonant frequency with the overlayer thickness H and f_0 means the resonance without overlayers. From Fig. 3(a), we can see that when all

the structures (free standing) shown in Fig. 1 are coated by an overlayer with dielectric constant of 3.0 and loss tangent of 0.02, the maximum frequency shifts can be obtained at the second resonance of the 2nd order SS-SRRs. Meanwhile it reveals that although two resonances can also be provided by the conventional SRRs when $E\perp$gap, the fractal SS-SRRs still have the advantage of higher sensitivity.

More intense electric field surrounding the sensor surface, when it is coated by overlayers, more frequency shifts will be induced.
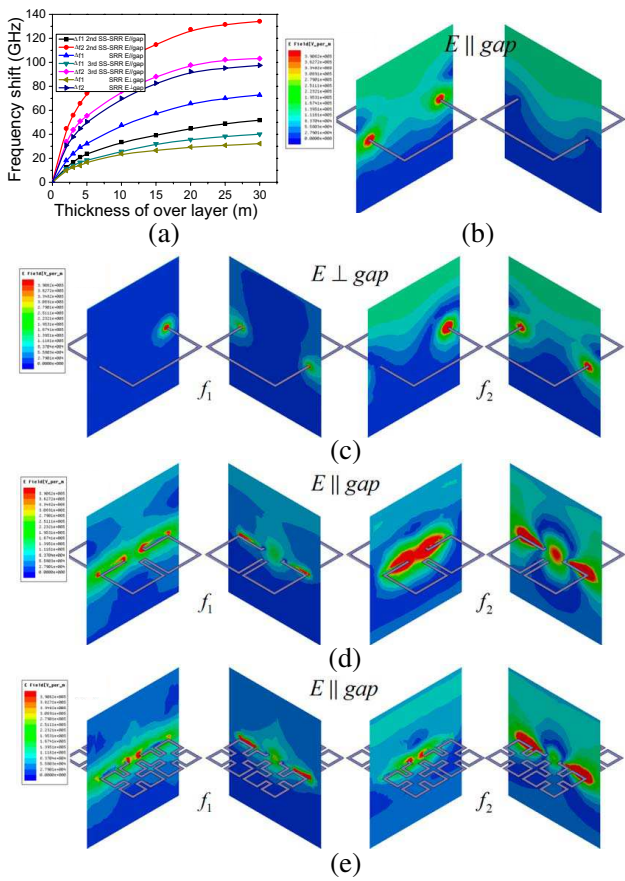

Figure 3. (a) Frequency shifts as a function of the overlayer thickness. (b) Cross-section view of the electric field penetration at the single resonance of convention SRR with $E//$gap. Cross-section view of the electric field penetration at two resonances of (c) conventional SRR with $E\perp$gap, (d) 2nd order SS-SRRs and (e) 3rd order SS-SRRs with $E//$gap.

Figs. 3(b)–(e) depict that maximum electric field intensity can be observed at the second resonance of the 2nd order SS-SRRs. So in this zone, disturbance caused by the thickness and permittivity of overlayers will induce maximum frequency shifts.

2.2. Influence of Different Geometrical Parameters

In order to analyze the influence of different geometrical parameters on the performance of SS-SRRs, length of inset Fd and Fs are varied. Fig. 4(a) shows simulated results of transmission spectra for the second-order SS-SRRs. The resonances shift to lower frequencies as Fd rises. The reason of this shift can be explained by the increased length of the strip. Fig. 4(b) shows the similar changing trend of transmission spectra for the third-order SS-SRRs. The first resonant frequency of the third-order SS-SRRs with the same value of $Fd = 40\,\mu m$ is lower than the second-order SS-SRRs due to the increase of the line length with increasing the fractal order. If further increasing the fractal order, more frequency shift can be expected.
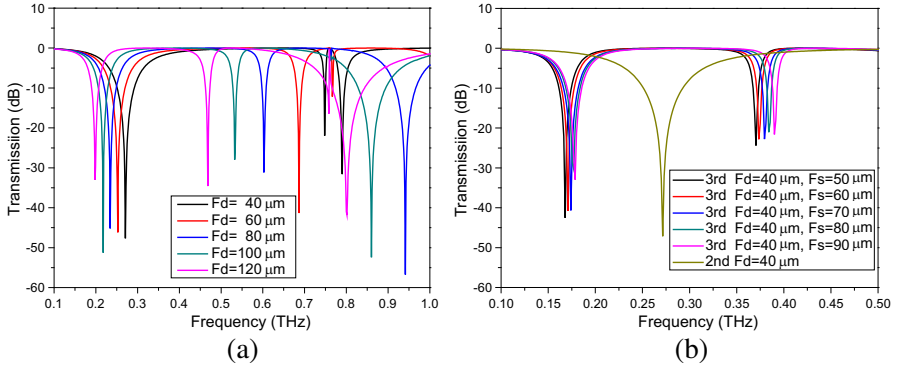

Figure 4. (a) Transmission response of second-order SS-SRRs for various inset length Fd. (b) Transmission response of third-order SS-SRRs for various Fs.

2.3. Influence of Different Overlayers

Fractal geometries shown in Figs. 1(b) and (c) are now coated by an overlayer with the dielectric constant of 3.0 and loss tangent of 0.02. Then the thickness of the overlayer is changed to investigate the characteristic of the MTM sensor. From the simulation results shown in Fig. 5, we can observe that if the thickness of the overlayer is less than $4\,\mu m$, the relation of Δf_H and H is approximately linearity.

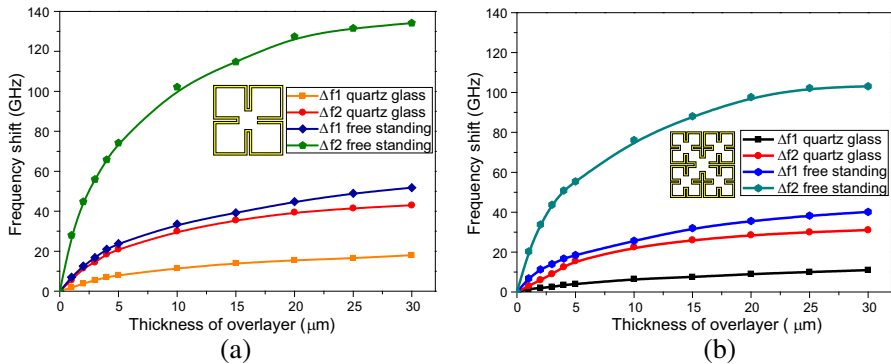**Figure 5.** Frequency shift as a function of the overlayer thickness for (a) the second-order SS-SRRs and (b) the third-order SS-SRRs.

Above 4 µm, the growth of frequency shift can be represented by a log linear trend. The shifting effect saturates at approximately 30 µm and no further significant shifts are observed. That is because the electric field falls off quickly away from the MTM layer and can be neglected above 30 µm. We can surmise that the SS-SRRs fringing fields extend out to roughly 30 µm. With the overlayer thickness of 30 µm, the second-order SS-SRRs sensor has maximum frequency shift of approximately 52 GHz and 134 GHz for the first resonant frequency and the second resonant frequency respectively.

When the MTM array is sustained by a thick or high-permittivity substrate, the electric field will mainly be bounded in the substrate. The electric flux outside of the substrate is weak and this substantially dilutes the change in frequency shift caused by the overlayers. As frequency shift is directly related with the sensitivity of the sensor, this phenomenon is considered as a limitation for MTM used for sensing. When the SS-SRRs sensor is backed by quartz glass with the thickness of 130 µm and permittivity of 3.75, the maximum sensitivity related to the second resonant frequency of the second order SS-SRRs decreases to the level of the first resonant frequency in free-standing case as shown in Fig. 5(a). Fig. 5(b) depicts that the similar tendency also happens to the third-order SS-SRRs.

Recently, there have been many studies focused on how to improve the sensitivity of MTM sensor and increase the percent change in the resonant frequency. In [22, 23], the direct write technique called proton beam writing (PBW) was used to fabricated high aspect ratio SRRs. In [24, 25], MTMs were fabricated on ultra-thin silicon nitride substrates. Both of the methods have been proven to have the ability to

enhance the sensitivity. We believe that if the two methods mentioned above are applied to the fractal structures used in this paper, the sensitivity can be further improved.

To explore the sensitivity to the dielectric constant of the unknown material, a similar procedure as in the previous examples can be applied. The relation between the frequency shifts and the dielectric constant of the overlayer with a constant thickness $H = 2\,\mu m$ is presented in Fig. 6. The frequency shift almost linearly increases with the dielectric constant increasing in the whole frequency range. This provides an effective method to probe the dielectric properties of the overlayer. From the Fig. 6, we can see that the second resonant frequency is more sensitive to the dielectric properties of the overlayer than the first resonant frequency and two-order SS-SRRs is more sensitive than the third-order SS-SRRs.
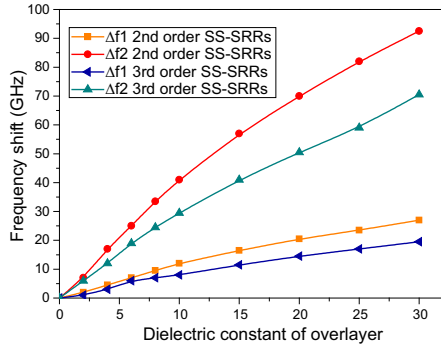

Figure 6. Frequency shift as a function of the dielectric constant of the overlayer coated on the SS-SRRs based on quartz glass with permittivity of 3.75 and thickness of 130 μm.

Since both the thickness and permittivity have effect on the frequency shift, the effect of thickness should be diminished when detecting the permittivity of unknown material with unknown thickness. As shown in Fig. 5, frequency shifts saturate beyond 30 μm. Under this occasion, the frequency shifts are only in relation with the permittivity of overlayers. In short, the overlayer should be beyond the saturated thickness when detecting its permittivity.

3. FABRICATION AND MEASUREMENT

The MTM were fabricated by conventional micro-fabrication techniques. 200 nm thick SS-SRRs structures made of Al were patterned on

quartz glass with thickness of 130 μm. Fig. 7 shows the photograph of a portion of the structure we have fabricated and tested. The transmission spectra were measured by the terahertz time-domain spectroscopy (TDS) system. In Figs. 8 and 9, we show how the measured spectra change as photoresist (Futurrex Inc., $\varepsilon_r = 2.7 \pm 0.2$ at 1.0 THz) is spun coated on the SS-SRRs. The thickness of overlayers is controlled by spin coating speed and time. For the second-order SS-SRRs, two resonant frequencies are observed at 0.1369 THz and 0.3424 THz without any overlayer coated. Then the TDS measurement was carried out on the spin-coated overlayer of photoresist with thickness of 2 μm, 4 μm, 10 μm. The resonances shift continuously to lower frequency as the thickness of the overlayer increased. Maximum shifts of 11.6 GHz and 37.8 GHz are observed for 10 μm thickness of photoresist, corresponding to 8.5% and 11% shift for the first resonant frequency and the second resonant frequency respectively. For the third-order SS-SRRs, the maximum shifts are 6.4 GHz and 21.3 GHz corresponding 6.2% and 9.2% shift for base resonances at 0.1033 THz and 0.2316 THz
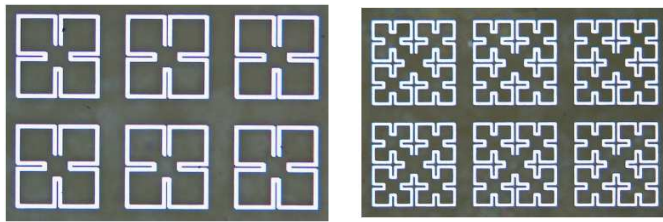

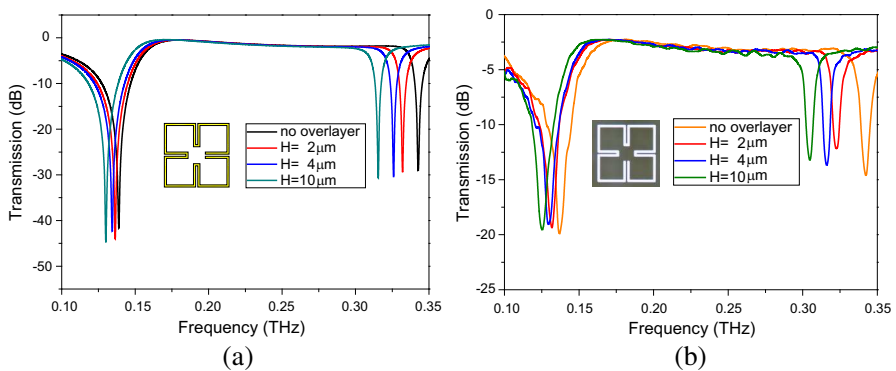**Figure 7.** Portions of optical microscope images of SS-SRRs.

Figure 8. (a) Simulated and (b) experimental transmission spectra of the second order SS-SRRs for various overlayers thickness.
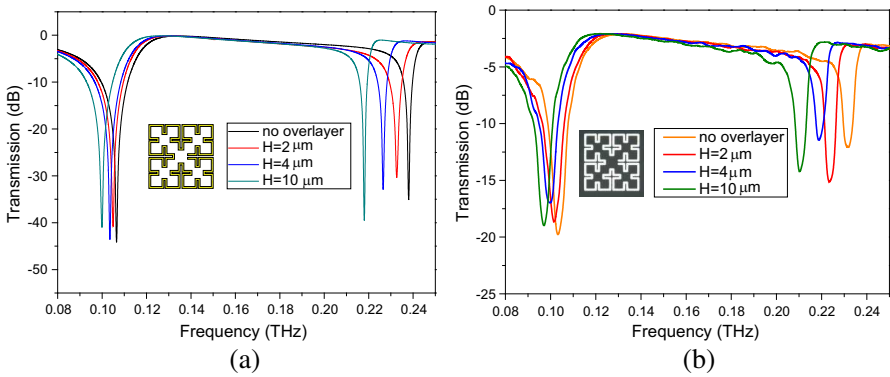
Figure 9. (a) Simulated and (b) experimental transmission spectra of the third order SS-SRRs for various overlayers thickness.

Table 1. Frequency shift of the SS-SRRs sensor for various overlayer thickness.

	2nd order SS-SRRs				3rd order SS-SRRs			
H (μm)	0	2	4	10	0	2	4	10
f_1 (THz)	0.1369	0.1317	0.1296	0.1253	0.1033	0.1015	0.0994	0.0969
f_2 (THz)	0.3424	0.3226	0.3161	0.3046	0.2316	0.2235	0.2192	0.2103
Δf_1 (GHz)	0	5.2	7.3	11.6	0	1.8	3.9	6.4
Δf_2 (GHz)	0	19.8	26.3	37.8	0	8.1	12.4	21.3

(f_1 denotes the first resonant frequency, f_2 denotes the second resonant frequency, Δf_1 and Δf_2 mean the frequency shifts.)

as list in Table 1. The simulated spectra have good agreement with experimental data. The small deviation is mainly due to the fabrication inaccuracy and the measurement error.

4. CONCLUSION

We have demonstrated numerically and experimentally the transmission characteristics of SRRs combined with a fractal square Sierpinski curve for terahertz sensing application. The transmission resonant fre-

quencies, owing to an increase in the area surrounded by metallic lines, decrease with an increase in the fractal order. We also investigate the frequency response when the SS-SRRs are coated with an overlayer of varying thickness and dielectric constant. Our results highlight the possibility of preparing more compact metamaterial sensor with dual-band operation and higher sensitivity. Measured results show good agreement with the simulated results. To further enhance the sensitivity, the structures mentioned in this study can also be fabricated on ultra-thin films such as SiN_X or with high aspect ratio SRRs, and this will be included in our future work.

ACKNOWLEDGMENT

REFERENCES

1. Ishimaru, A., S. Jaruwatanadilok, and Y. Kuga, "Generalized surface plasmon resonance sensors using metamaterials and negative index materials," *Progress In Electromagnetics Research*, Vol. 51, 139–152, 2005.

2. Smith, D. R., W. J. Padilla, D. Vier, S. C. Nemat-Nasser, and S. Schultz, "Composite medium with simultaneously negative permeability and permittivity," *Phys. Rev. Lett.*, Vol. 84, No. 18, 4184–4187, 2000.

3. He, X., Y. Wang, J. Wang, and T. Gui, "Thin-film sensor based tip-shaped split ring resonator metamaterial for microwave application," *Microsyst. Technol.*, Vol. 16, No. 10, 1735–1739, 2010.

4. Kanté, B., D. Germain, and A. De Lustrac, "Experimental demonstration of a nonmagnetic metamaterial cloak at microwave frequencies," *Phys. Rev. B*, Vol. 80, No. 20, 201104, 2009.

5. La Spada, L., F. Bilotti, and L. Vegni, "Metamaterial-based sensor design working in infrared frequency range," *Progress In Electromagnetics Research B*, Vol. 34, 205–223, 2011.

6. Lee, H. M. and H. Lee, "A dual-band metamaterial absorber based with resonant-magnetic structures," *Progress In Electromagnetics Research Letters*, Vol. 33, 1–12, 2012.

7. Kuznetsov, S. A., A. G. Paulish, A. V. Gelfand, P. A. Lazorskiy, and V. N. Fedorinin, "Matrix structure of metamaterial absorbers for multispectral terahertz imaging," *Progress In Electromagnetics Research*, Vol. 122, 93–103, 2012.

8. Huang, L. and H. Chen, "Multi-band and polarization insensitive metamaterial absorber," *Progress In Electromagnetics Research*, Vol. 113, 103–110, 2011.

9. Pendry, J. B., "Negative refraction makes a perfect lens," *Phys. Rev. Lett.*, Vol. 85, No. 18, 3966–3969, 2000.

10. Meng, F. Y., Y. L. Li, K. Zhang, Q. Wu, and J. L. W. Li, "A detached zero index metamaterial lens for antenna gain enhancement," *Progress In Electromagnetics Research*, Vol. 132, 463–478, 2012.

11. Gong, Y. and G. Wang, "Superficial tumor hyperthermia with flat left-handed metamaterial lens," *Progress In Electromagnetics Research*, Vol. 98, 389–405, 2009.

12. Siegel, P. H., "Terahertz technology in biology and medicine," *IEEE Trans. on Microwave Theory and Tech.*, Vol. 52, No. 10, 2438–2447, 2004.

13. Withayachumnankul, W. and D. Abbott, "Metamaterials in the terahertz regime," *IEEE Photon. J.*, Vol. 1, No. 2, 99–118, 2009.

14. Tao, H., W. J. Padilla, X. Zhang, and R. D. Averitt, "Recent progress in electromagnetic metamaterial devices for terahertz applications," *IEEE J. Sel. Top. Quantum Electron.*, Vol. 17, No. 1, 92–101, 2011.

15. Miyamaru, F., Y. Saito, M. Takeda, B. Hou, L. Liu, W. Wen, et al., "Terahertz electric response of fractal metamaterial structures," *Phys. Rev. B.*, Vol. 77, No. 4, 045124, 2008.

16. Miyamaru, F., S. Kubota, and M. W. Takeda, "Optics express optics letters," *Appl. Phys. Express*, Vol. 5, No. 7, 2001, 2012.

17. De la Mata Luque, T. M., N. R. K. Devarapalli, and C. G. Christodoulou, "Investigation of bandwidth enhancement in volumetric left-handed metamaterials using fractals," *Progress In Electromagnetics Research*, Vol. 131, 185–194, 2012.

18. O'Hara, J. F., W. Withayachumnankul, and I. Al-Naib, "A review on thin-film sensing with terahertz waves," *J. Infrared Millim. Terahertz Waves*, Vol. 33, 245–291, 2012.

19. Bingham, C. M., H. Tao, X. Liu, R. D. Averitt, X. Zhang, and W. J. Padilla, "Planar wallpaper group metamaterials for novel terahertz applications," *Opt. Express*, Vol. 16, No. 23, 18565–18575, 2008.

20. Padilla, W. J., A. J. Taylor, C. Highstrete, M. Lee, and R. D. Averitt, "Dynamical electric and magnetic metamaterial response at terahertz frequencies," *Phys. Rev. Lett.*, Vol. 96, No. 10, 107401, 2006.

21. Miyamaru, F., Y. Saito, M. Takeda, L. Liu, B. Hou, W. Wen, et al., "Emission of terahertz radiations from fractal antennas," *Appl. Phys. Lett.*, Vol. 95, No. 22, 221111–221111-3, 2009.

22. Chiam, S. Y., R. Singh, J. Gu, J. Han, W. Zhang, and A. A. Bettiol, "Increased frequency shifts in high aspect ratio terahertz split ring resonators," *Appl. Phys. Lett.*, Vol. 94, No. 6, 064102–064102-3, 2009.

23. Chiam, S. Y., R. Singh, W. Zhang, and A. A. Bettiol, "Controlling metamaterial resonances via dielectric and aspect ratio effects," *Appl. Phys. Lett.*, Vol. 97, No. 19, 191906–191906-3, 2010.

24. Tao, H., A. C. Strikwerda, M. Liu, J. P. Mondia, E. Ekmekci, K. Fan, et al., "Performance enhancement of terahertz metamaterials on ultrathin substrates for sensing applications," *Appl. Phys. Lett.*, Vol. 97, No. 26, 261909–261909-3, 2010.

25. Tao, H., A. Strikwerda, K. Fan, C. Bingham, W. Padilla, X. Zhang, et al., "Terahertz metamaterials on free-standing highly-flexible polyimide substrates," *J. Phys. D: Appl. Phys.*, Vol. 41, 232004, 2008.